

Supplementary Information

**Magnetic dynamics in an open-ring tridysprosium complex
employing mixed ligands**

Si-Guo Wu,^a Yuan-Yuan Peng,^a Yan-Cong Chen,^a and Jun-Liang Liu^{*a} and Ming-Liang Tong^a

^a Key Laboratory of Bioinorganic and Synthetic Chemistry of Ministry of Education, School of Chemistry,
Sun Yat-Sen University, 510275 Guangzhou, Guangdong, P. R. China.

Crystal Data and Structures

Table S1. The selected bond length (Å) and bond angle (°) for **1**.

Bond length	Bond angle
Dy1-O10	2.299(4)
Dy1-O11	2.342(4)
Dy1-O13	2.265(4)
Dy1-O14	2.299(5)
Dy1-N5	2.529(6)
Dy1-N6	2.521(6)
Dy1-N7	2.515(6)
Dy1-N8	2.532(6)
Dy2-O4	2.476(4)
Dy2-O5	2.314(5)
Dy2-O6	2.576(5)
Dy2-O7	2.247(5)
Dy2-O8	2.234(5)
Dy2-O9	2.563(5)
Dy2-O10	2.311(4)
Dy2-O11	2.436(4)
Dy3-O1	2.279(5)
Dy3-O2	2.293(5)
Dy3-O4	2.334(5)
Dy3-O5	2.295(4)
Dy3-N1	2.504(6)
Dy3-N2	2.547(6)
Dy3-N3	2.546(7)
Dy3-N4	2.513(6)
O10-Dy1-O11	69.60(15)
O10-Dy1-O14	137.77(17)
O10-Dy1-N5	78.24(17)
O10-Dy1-N6	83.25(16)
O10-Dy1-N7	105.79(18)
O10-Dy1-N8	70.22(18)
O11-Dy1-N5	70.04(17)
O11-Dy1-N6	131.21(18)
O11-Dy1-N7	86.48(18)
O11-Dy1-N8	120.49(17)
O13-Dy1-O10	149.60(17)
O13-Dy1-O11	81.22(16)
O13-Dy1-O14	72.60(18)
O13-Dy1-N5	84.07(19)
O13-Dy1-N6	111.39(18)
O13-Dy1-N7	80.0(2)
O13-Dy1-N8	135.52(19)
O14-Dy1-O11	150.40(17)
O14-Dy1-N5	119.38(18)
O14-Dy1-N6	72.91(19)
O14-Dy1-N7	75.74(19)
O14-Dy1-N8	73.01(19)
N5-Dy1-N8	138.09(19)
N6-Dy1-N5	65.09(18)
N6-Dy1-N8	84.05(19)
N7-Dy1-N5	153.39(19)
N7-Dy1-N6	141.0(2)
N7-Dy1-N8	64.8(2)
O4-Dy2-O6	114.33(15)
O4-Dy2-O9	75.62(16)
O5-Dy2-O4	68.10(15)
O5-Dy2-O6	62.47(16)
O5-Dy2-O9	77.65(16)
O5-Dy2-O11	130.57(15)
O7-Dy2-O4	78.03(16)
O7-Dy2-O5	142.46(16)
O7-Dy2-O6	151.82(17)
O7-Dy2-O9	78.73(17)
O7-Dy2-O10	113.92(16)
O7-Dy2-O11	86.03(16)
O8-Dy2-O4	83.61(16)
O8-Dy2-O5	114.95(17)

O8-Dy2-O6	80.85(16)
O8-Dy2-O7	75.35(17)
O8-Dy2-O9	149.58(17)
O8-Dy2-O10	144.00(16)
O8-Dy2-O11	78.80(16)
O9-Dy2-O6	127.93(16)
O10-Dy2-O4	131.72(15)
O10-Dy2-O5	79.75(15)
O10-Dy2-O6	77.78(15)
O10-Dy2-O9	62.64(16)
O10-Dy2-O11	67.79(15)
O11-Dy2-O4	158.77(15)
O11-Dy2-O6	74.61(15)
O11-Dy2-O9	115.14(16)
O1-Dy3-O2	72.61(19)
O1-Dy3-O4	149.96(17)
O1-Dy3-O5	136.69(18)
O1-Dy3-N1	74.73(19)
O1-Dy3-N2	119.80(18)
O1-Dy3-N3	73.6(2)
O1-Dy3-N4	75.66(19)
O2-Dy3-O4	81.05(17)
O2-Dy3-O5	150.66(17)
O2-Dy3-N1	112.90(18)
O2-Dy3-N2	83.83(18)
O2-Dy3-N3	135.7(2)
O2-Dy3-N4	79.7(2)
O4-Dy3-N1	130.37(19)
O4-Dy3-N2	70.05(17)
O4-Dy3-N3	119.46(17)
O4-Dy3-N4	85.83(18)
O5-Dy3-O4	70.91(16)
O5-Dy3-N1	80.69(18)
O5-Dy3-N2	78.76(17)
O5-Dy3-N3	68.90(18)
O5-Dy3-N4	105.98(19)
N1-Dy3-N2	65.0(2)
N1-Dy3-N3	84.40(19)
N1-Dy3-N4	142.0(2)
N3-Dy3-N2	138.6(2)
N4-Dy3-N2	152.7(2)
N4-Dy3-N3	64.7(2)

Table S2. Continuous shape measures calculations (CShM)^{1,2} for rare-earth ions in **1** and **2**.

Complex	OP-8	HPY-8	HBPY-8	CU-8	SAPR-8	TDD-8	JGBF-8
Dy1	30.10	21.76	15.48	10.15	1.25	2.65	14.57
Dy2	29.25	23.69	16.68	10.95	1.22	3.53	15.73
Dy3	29.84	21.74	15.44	9.84	1.19	2.85	14.58
JETBPY-8 JBTPR-8 BTPR-8 JSD-8 TT-8 ETBPY-8							
Dy1	23.44	2.95	2.40	4.80	10.69	19.78	
Dy2	23.10	3.16	3.13	4.91	11.76	19.66	
Dy3	23.49	2.95	2.37	4.95	10.37	19.84	

OP-8 = Octagon (D_{8h}); HPY-8 = Heptagonal pyramid (C_{7v}); HBPY-8 = Hexagonal bipyramid (D_{6h}); CU-8 = Cube (O_h); SAPR-8 = Square antiprism (D_{4d}); TDD-8 = Triangular dodecahedron (D_{2d}); JGBF-8 = J Johnson gyrobifastigium J26 (D_{2d}). JETBPY-8 = Johnson elongated triangular bipyramid J14 (D_{3h}); JBTPR-8 = Biaugmented trigonal prism J50 (C_{2v}); BTPR-8 = Biaugmented trigonal prism (C_{2v}); JSD-8 = Snub diphenoïd J84 (D_{2d}); TT-8 = Triakis tetrahedron (T_d) and ETBPY-8 = Elongated trigonal bipyramid (D_{3h}).

[1] Alvarez, S.; Alemany, P.; Casanova, D.; Cirera, J.; Llunell, M.; Avnir, D. Shape maps and polyhedral interconversion paths in transition metal chemistry. *Coord. Chem. Rev.* **2005**, 249 (17), 1693-1708.

[2] Casanova, D.; Llunell, M.; Alemany, P.; Alvarez, S. The Rich Stereochemistry of Eight-Vertex Polyhedra: A Continuous Shape Measures Study. *Chem. Eur. J.* **2005**, 11 (5), 1479-1494.

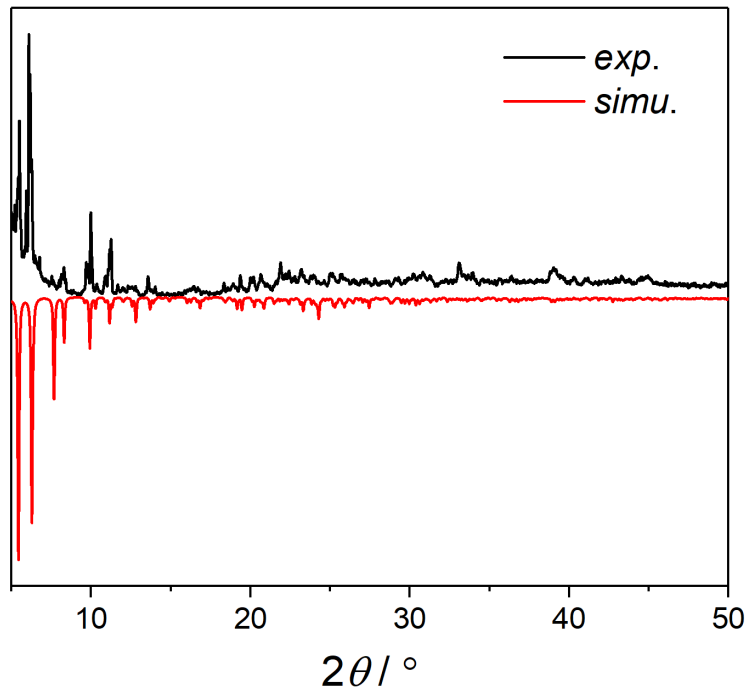


Figure S1. The experimental and simulated powder X-ray diffraction (PXRD) patterns for **1**.

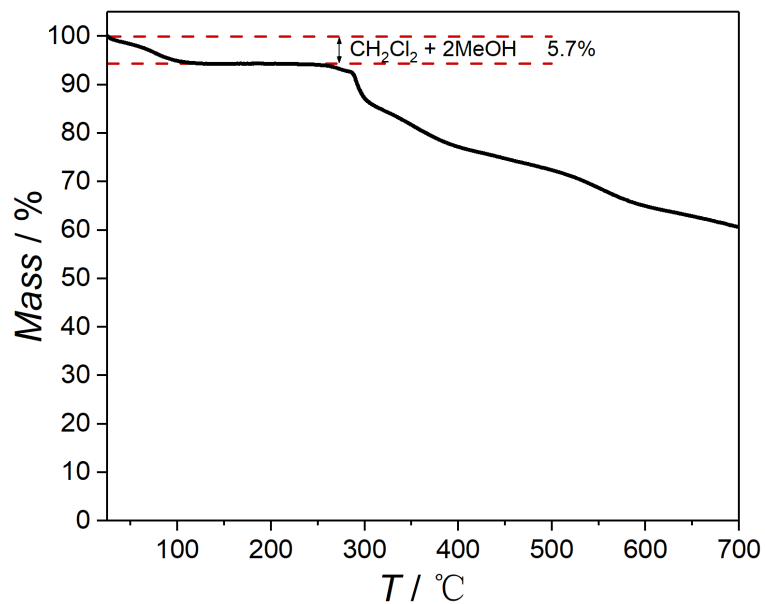


Figure S2. Thermogravimetric analysis (TGA) curve at a heating rate of 10 K min^{-1} . Exptl. ($200 {}^\circ\text{C}$): 5.7%, calc: 5.7%.

Magnetic Characterization

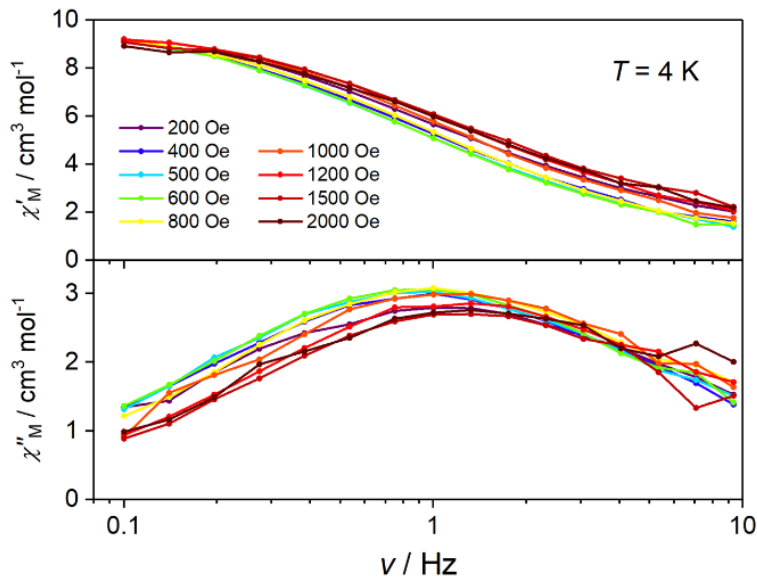


Figure S3. Frequency-dependence of the in-phase product (χ'_M) and out-of-phase (χ''_M) at 4 K under 0–2 kOe dc field for **1**.

Table S3. The best-fit parameters obtained from the generalized Debye model at zero dc field.

T / K	χ_0 / $\text{cm}^3 \text{ mol}^{-1}$	χ_∞ / $\text{cm}^3 \text{ mol}^{-1}$	τ / s	α	R^2
2	23.29088	0.90336	1.29938	0.48437	0.99665
3	14.64284	0.75402	0.38529	0.43399	0.99755
4	10.50752	0.64213	0.13306	0.37506	0.9984
5	8.2069	0.55028	0.05086	0.3158	0.99897
6	6.79868	0.46771	0.02252	0.2763	0.99939
7	5.92623	0.37295	0.01175	0.26609	0.99967
8	5.15296	0.32737	0.00647	0.24298	0.99974
9	4.56045	0.29189	0.00386	0.22611	0.99976
10	4.09587	0.26518	0.00245	0.21378	0.99968
11	3.71955	0.25164	0.00163	0.20177	0.99962
12	3.37491	0.23164	0.00106	0.19501	0.99962
13	3.12871	0.2201	7.49304E-4	0.19136	0.9996
14	2.90814	0.21222	5.31377E-4	0.1857	0.99965
15	2.71485	0.23359	3.86419E-4	0.17616	0.99965
16	2.54256	0.24705	2.79308E-4	0.1669	0.99967
17	2.39545	0.25919	2.01906E-4	0.16437	0.99974
18	2.25538	0.26251	1.44327E-4	0.14923	0.99979
19	2.13429	0.28927	1.03925E-4	0.13967	0.99981
20	2.03082	0.23448	7.16994E-5	0.13189	0.99988

Table S4. The best-fit parameters obtained from the generalized Debye model at 500 Oe dc field.

T / K	$\chi_0 / \text{cm}^3 \text{ mol}^{-1}$	$\chi_\infty / \text{cm}^3 \text{ mol}^{-1}$	τ / s	α	R^2
2	18.5201	0.28902	1.60361	0.39095	0.99884
3	12.03296	0.25634	0.47415	0.3576	0.99931
4	8.91401	0.22728	0.1688	0.31792	0.99948
5	7.04549	0.20654	0.06642	0.27843	0.99959
6	5.85907	0.18309	0.03015	0.25515	0.99952
7	5.12926	0.13518	0.01598	0.2605	0.99974
8	4.49526	0.12279	0.00893	0.24632	0.9994
9	3.97982	0.1047	0.00529	0.24211	0.99962
10	3.56376	0.10168	0.0033	0.23165	0.99955
11	3.23829	0.1069	0.00217	0.21949	0.99941
12	2.93218	0.10022	0.00139	0.2137	0.99921
13	2.70557	0.11666	9.58452E-4	0.19933	0.99928
14	2.52204	0.13252	6.77485E-4	0.18919	0.99926
15	2.35352	0.13169	4.71963E-4	0.1858	0.99933
16	2.20192	0.16378	3.37349E-4	0.16895	0.99921
17	2.06659	0.15552	2.33524E-4	0.1685	0.99942
18	1.95322	0.19121	1.69801E-4	0.15189	0.99941
19	1.84871	0.17935	1.16792E-4	0.14408	0.99972
20	1.74904	0.21125	8.40138E-5	0.1206	0.99957

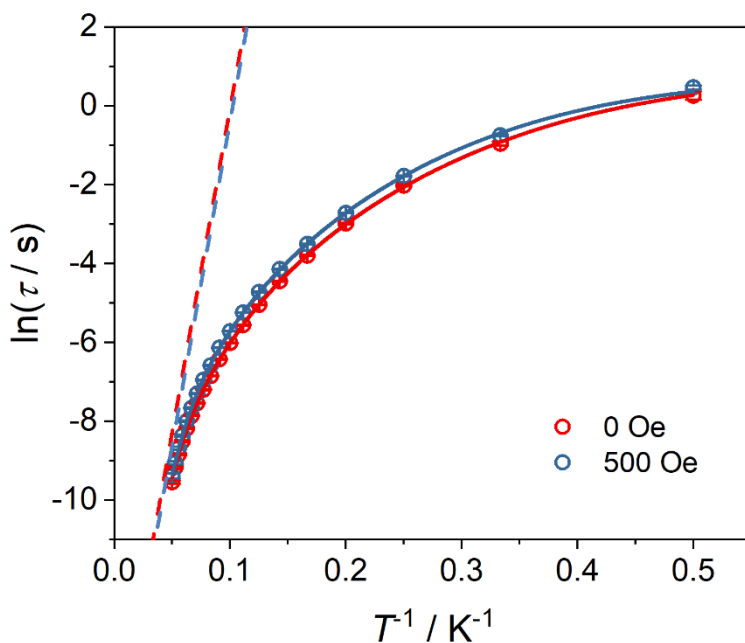


Figure S4. The relaxation time versus T plots for **1**. The solid lines are the best fit with equation $\tau^{-1} = \tau_0^{-1}\exp(-U_{\text{eff}}/k_B T) + CT^n + \tau_{\text{QTM}}^{-1}$ and gives a share $U_{\text{eff}} = 114(7) \text{ cm}^{-1}$. The dashed line represents for the tendency of the Orbach-type process.

***Ab initio* calculation**

Computational Details. *Ab initio* calculations were performed with OpenMOLCAS version 18.09¹ and are of the CASSCF/RASSI type. The Cholesky decomposition threshold was set to 1×10^{-8} to save disk space. An entire molecule was included, and the coordinates of atoms were extracted from the experimentally determined crystal structure. The adjacent Dy(III) sites were computationally replaced by the diamagnetic Y(III). ANO-RCC basis set approximations have been employed (see Table S4).²⁻³ Active space of the CASSCF method included nine electrons in seven 4f orbitals of Dy(III). 21 sextets for Dy(III) were optimized in state-averaged calculations and then mixed by spin-orbit coupling using RASSI approach.⁴ The g-tensors, energy spectra, main magnetic axis as well as the magnetizations were obtained by SINGLE_ANISO routine⁵.

- [1] Aquilante, F.; Autschbach, J.; Carlson, R. K.; Chibotaru, L. F.; Delcey, M. G.; De Vico, L.; Fdez. Galván, I.; Ferré, N.; Frutos, L. M.; Gagliardi, L.; Garavelli, M.; Giussani, A.; Hoyer, C. E.; Li Manni, G.; Lischka, H.; Ma, D.; Malmqvist, P. Å.; Müller, T.; Nenov, A.; Olivucci, M.; Pedersen, T. B.; Peng, D.; Plasser, F.; Pritchard, B.; Reiher, M.; Rivalta, I.; Schapiro, I.; Segarra-Martí, J.; Stenrup, M.; Truhlar, D. G.; Ungur, L.; Valentini, A.; Vancoillie, S.; Veryazov, V.; Vysotskiy, V. P.; Weingart, O.; Zapata, F.; Lindh, R. Molcas 8: New capabilities for multiconfigurational quantum chemical calculations across the periodic table. *J. Comput. Chem.* 2016, 37 (5), 506-541.
- [2] Roos, B. O.; Lindh, R.; Malmqvist, P.-Å.; Veryazov, V.; Widmark, P.-O.; Borin, A. C. New Relativistic Atomic Natural Orbital Basis Sets for Lanthanide Atoms with Applications to the Ce Diatom and LuF3. *J. Phys. Chem. A* 2008, 112 (45), 11431-11435.
- [3] Roos, B. O.; Lindh, R.; Malmqvist, P.-Å.; Veryazov, V.; Widmark, P.-O. Main group atoms and dimers studied with a new relativistic ANO basis set. *J. Phys. Chem. A* 2004, 108 (15), 2851-2858.
- [4] Malmqvist, P. Å.; Roos, B. O.; Schimmelpfennig, B. The restricted active space (RAS) state interaction approach with spin-orbit coupling. *Chem. Phys. Lett.* 2002, 357 (3), 230-240.
- [5] Chibotaru, L. F.; Ungur, L. Ab initio calculation of anisotropic magnetic properties of complexes. I. Unique definition of pseudospin Hamiltonians and their derivation. *J. Chem. Phys.* 2012, 137 (6), 064112.

Table S5. The employed ANO-RCC basis sets.

1	
	Dy.ANO-RCC-VTZP
	Y.ANO-RCC-VDZP
ANO-RCC basis sets	O.ANO-RCC-VDZ
	N.ANO-RCC-VDZ
	C.ANO-RCC-VDZ
	H.ANO-RCC-MB

Table S6. The energy spectra and g tensors for the eight Kramers doublets of the $^6H_{15/2}$ multiplets for Dy(III) ions in **1**.

	E / cm^{-1}	g_x	g_y	g_z
Dy1	0	0.0083	0.0165	19.608
	133.4008	0.1560	0.2081	16.664
	220.7048	0.6559	0.8775	13.117
	325.8642	2.2202	3.7194	9.8892
	412.2692	2.6040	4.5305	11.615
	463.8032	0.0826	2.7287	12.830
	549.0074	0.6856	1.8792	16.256
Dy2	618.3796	0.3139	1.0819	18.449
	0	0.0099	0.0223	19.718
	122.1173	0.073	0.2369	16.874
	186.187	1.2241	2.9802	13.428
	221.292	1.8994	5.3407	10.249
	264.3722	1.1340	4.4627	10.897
	326.0537	1.9312	2.0886	14.726
Dy3	445.2158	0.1473	0.1628	17.081
	652.4321	0.0030	0.0040	19.260
	0	0.0079	0.0146	19.642
	125.0711	0.1299	0.1614	16.816
	214.6793	0.4435	0.6240	13.255
	315.2309	1.9627	3.1608	10.152
	389.1664	3.2829	4.1635	13.495
	451.2692	1.1047	2.3024	12.228
	526.8271	0.9981	2.6851	16.147
	617.5835	0.2344	0.7171	18.988